Use of NanoBiT and NanoBRET to monitor fluorescent VEGF-A binding kinetics to VEGFR2/NRP1 heteromeric complexes in living cells.

Chloe Peach[1], Laura Kilpatrick[1], Jeanette Woolard[1], and Stephen Hill[1]

[1]University of Nottingham

August 27, 2020

Abstract

Background: Vascular Endothelial Growth Factor A (VEGF-A) is a key mediator of angiogenesis, primarily signalling via VEGF Receptor 2 (VEGFR2). Endothelial cells also express the co-receptor Neuropilin-1 (NRP1) that potentiates VEGF-A/VEGFR2 signalling. VEGFR2 and NRP1 had distinct real-time ligand binding kinetics when monitored using Bioluminescence Resonance Energy Transfer (BRET). We previously characterised fluorescent VEGF-A isoforms tagged at a single site with tetramethylrhodamine (TMR). Here, we explore differences between VEGF-A isoforms in living cells that co-expressed both receptors. Experimental Approach: Receptor localisation was monitored in HEK293T cells expressing both VEGFR2 and NRP1 using a membrane-impermeant HaloTag and SnapTag technologies. To isolate ligand binding pharmacology at a defined VEGFR2/NRP1 complex, we developed an assay using NanoBiT complementation technology whereby heteromerization is required for luminescence emissions. Binding affinities and kinetics of VEGFR2-selective VEGF165b-TMR and non-selective VEGF165a-TMR were monitored using BRET from this defined complex. Key Results: Cell surface VEGFR2 and NRP1 were co-localised and formed a constitutive heteromeric complex. Despite being selective for VEGFR2, VEGF165b-TMR had a distinct kinetic ligand binding profile at the complex that largely remained elevated in cells over 90 minutes. VEGF165a-TMR bound to the VEGFR2/NRP1 complex with kinetics comparable to those of VEGFR2 alone. Using a binding-dead mutant of NRP1 had no impact on the binding kinetics or affinity of VEGF165a-TMR. Conclusions and Implications: This NanoBiT approach enabled real-time ligand binding to be quantified in living cells at 37°C from a specified complex between a receptor tyrosine kinase and its co-receptor for the first time.

INTRODUCTION

Angiogenesis involves the growth of new blood vessels from existing vascular networks (Carmeliet, 2005). This important physiological process can also be dysregulated in numerous pathologies, such as in tumour development (Chung and Ferrara, 2011). Vascular endothelial growth factor A (VEGF-A) is a key mediator of angiogenesis that primarily signals via its cognate receptor tyrosine kinase (RTK), the VEGF Receptor 2 (VEGFR2) (Simons et al., 2016; Peach et al., 2018b). VEGF-A binds across immunoglobulin-like domains 2 and 3 of VEGFR2 (Ruch et al., 2007; Leppanen et al., 2010). Agonist binding results in conformational changes throughout the VEGFR2 dimer that lead to auto- and trans-phosphorylation of key intracellular tyrosine residues. This triggers numerous signalling cascades that ultimately initiate endothelial cell proliferation, migration and survival, as well as increased vascular permeability (Koch et al., 2011).

VEGFR2 is subject to complex trafficking via clathrin-dependent and clathrin-independent endocytosis (Ewan et al., 2006; Basagiannis and Christoforidis, 2016; Basagiannis et al., 2016). It internalises in both the presence and absence of VEGF-A (Ewan et al., 2006; Jopling et al., 2009; Jopling et al., 2011). VEGF-A can

also bind to the VEGFR2 co-receptor Neuropilin-1 (NRP1), a type 1 transmembrane glycoprotein (Soker et al., 1998, 2002). VEGFR2 signalling is upregulated by NRP1 (Fantin et al., 2011; Djordjevic and Driscoll, 2013; Gelfand et al., 2014). Endothelial cells express both VEGFR2 and NRP1 (Soker et al., 1998; Witmer et al., 2002). NRP1 is also overexpressed in numerous tumour subtypes (Jubb et al., 2012; Goel and Mercurio, 2013; Lee et al., 2014) and immune cells in the tumour microenvironment (Roy et al., 2017). VEGF-A interacts with VEGFR2 via residues encoded at the N-terminus of VEGF-A (Leppanen et al., 2010; Brozzo et al., 2011), while the C-terminus can interact with NRP1 (Mamluk et al., 2002; Vander Kooi et al., 2007; Parker et al., 2012).

VEGF-A is an anti-parallel, disulphide-linked homodimer. Alternative splicing of VEGF-A mRNA leads to a number of distinct VEGF-A isoforms (Woolard et al., 2009; Peach et al., 2018b). VEGF-A isoforms have different signalling properties in physiological systems with distinct expression profiles in health and disease (Vempati et al., 2014). VEGF-A isoforms differ in length, such as pro-angiogenic $VEGF_{165}a$ or the shorter $VEGF_{121}a$ isoform. A major site of splicing occurs at exon 8, where proximal splicing results in $VEGF_{xxx}a$ isoforms that contain exon 8a-encoded residues (CDKPRR) and $VEGF_{xxx}b$ isoforms that instead contain exon 8b-encoded residues (SLTKDD). While $VEGF_{165}a$ stimulates angiogenesis as a full agonist, $VEGF_{165}b$ is a partial agonist with reported anti-angiogenic activity *in vivo* (Woolard et al., 2004; Cébe Suarez et al., 2006; Eswarappa et al., 2014). The b1 domain of NRP1 can interact with $VEGF_{165}a$ via an arginine residue encoded by exon 8a (Mamluk et al., 2002; Vander Kooi et al., 2007; Parker et al., 2012). In contrast, 'anti-angiogenic' $VEGF_{165}b$ isoforms are unable to interact with NRP1 (Cébe Suarez et al., 2006; Kawamura et al., 2008; Delcombel et al., 2013).

Fluorescence-based technologies have been used to advance our pharmacological understanding of G protein-coupled receptors (GPCRs), RTKs and other classes of membrane protein (Stoddart et al., 2017). For example, Bioluminescence Resonance Energy Transfer (BRET) is a proximity-based assay that can quantify real-time binding at 37°C in living cells (Stoddart et al., 2015). A receptor is tagged at the N-terminus with a 19 kDa NanoLuciferase (NanoLuc) such that NanoLuc emits luminescence upon oxidation of the furimazine substrate. This can excite a nearby fluorophore in close proximity (<10 nm), such as a compatible fluorescent ligand bound at the receptor's orthosteric site. We previously developed fluorescent VEGF-A isoforms that were single-site labelled with tetramethylrhodamine (TMR), to monitor ligand binding at full-length VEGFR2 or NRP1 tagged with NanoLuc (Kilpatrick et al., 2017; Peach et al., 2018a, 2019). Despite having a similar nanomolar binding affinity, $VEGF_{165}a$-TMR binding kinetics were significantly faster at NRP1 than VEGFR2 (Peach et al., 2018a). VEGFR2 and NRP1 were also subject to distinct subcellular trafficking in the absence or presence of ligand when expressed alone. These techniques were limited to quantifying protein-protein interactions at NanoLuc-tagged VEGFR2 or NRP1 expressed in isolation, however endothelial cells and tumour cells endogenously express both VEGFR2 and NRP1 in the same cell (Whitaker et al., 2001; Prahst et al., 2008; Fantin et al., 2013; Koch et al., 2014; Lee-Montiel et al., 2015). Since these receptors have distinct ligand binding dynamics and subcellular localisation, approaches are required that isolate the pharmacology of VEGF-A ligand binding to distinct complexes involving both VEGFR2 and NRP1.

NanoLuc Binary Technology (NanoBiT) uses a modified NanoLuc split into a large fragment (LgBiT; 156 amino acids) and a small 11 amino acid tag (HiBiT or SmBiT; Dixon et al., 2016). Complementation of fragments is required for luminescence emission. Numerous variants were developed of the small tag with different intrinsic affinities for complementation with the LgBiT fragment, including the 'higher affinity' HiBiT fragment (K_d ~0.7 nM) and the lower affinity SmBiT fragment (K_d ~190 μM). Used in combination with a fluorescent ligand, interactions between the ligand and a particular protein pairing can be monitored using NanoBiT and BRET. Here we have used this technology to investigate the kinetics of ligand binding of $VEGF_{165}a$-TMR (Kilpatrick et al., 2017) and $VEGF_{165}b$-TMR (Peach et al., 2018a) to oligomeric complexes containing both VEGFR2 and NRP1.

METHODS

Cell Culture and Materials

HEK293T cells (CCLV Cat# CCLV-RIE 1018, RRID:CVCL_0063) were maintained at 37°C/5% CO_2 in Dulbecco's Modified Eagle's Medium (DMEM; Sigma-Aldrich, USA) supplemented with 10% Fetal Calf Serum (FCS; Sigma-Aldrich, USA). For a consistent cell background with functional studies performed using a reporter gene assay, all HEK293T cells also expressed a Firefly luciferase reporter gene (RE-Luc2P) that was inserted downstream of the NFAT promoter. Control experiments confirmed that HEK293T-NFAT-ReLuc2P cells did not emit luminescence in response to furimazine alone that interfered with NanoBiT or NanoBRET assays. Cells were passaged at 70-80% confluency using phosphate buffered saline (PBS; Lonza, Switzerland) and trypsin (0.25% w/v in versene; Lonza). Fluorescent $VEGF_{165}$a and $VEGF_{165}$b were labelled at a single N-terminal cysteine residue with TMR using the HaloTag mammalian protein detection and purification system (G6795; Promega Corporation, USA) as described previously (Kilpatrick et al., 2017; Peach et al., 2018a). Fluorescent ligands were characterised in terms of labelling efficiency, dimerisation and function as described in Kilpatrick et al. (2017) and Peach et al. (2018a). Ligands were stored at -20°C in 2.5mg/ml protease-free bovine serum albumin (BSA; Millipore, USA). Unlabelled recombinant human VEGF isoforms were purchased from R&D Systems (Abingdon, UK). Furimazine and purified NanoBiT fragments were purchased from Promega Corporation (Madison, USA).

Generating Constructs

N-terminal NanoLuc-tagged VEGFR2 (NM_002253) and NRP1 (NM_003873.5) were cloned in a pFN31K vector encoding the secretory IL-6 signal peptide fused to the N-terminus of NanoLuc, followed by a GSS-GAIA linker before the receptor. HaloTag-VEGFR2 and HaloTag-NRP1 were cloned in a pFN21A vector with the IL-6 signal peptide followed by a sequence encoding HaloTag and an EPTTEDLYFQSDNAIA linker at the receptor N-terminus. SnapTag-NRP1 was cloned into a pcDNA3.1 vector encoding a murine 5HT3A signal sequence followed by the SnapTag and a STSPVWWNSADIQHSGGRSSGAIA linker. The receptor-encoded sequence from NanoLuc-NRP1 vector was used to generate SnapTag-NRP1 using the XhoI and XbaI restriction sites. N-terminal LgBiT-VEGFR2 and LgBiT-NRP1 were cloned in the pFN21A vector with the IL-6 signal peptide, LgBiT sequence and a flexible GSSGGGGSGGGGSSGGAIA linker. The LgBiT tag sequence from N198A pBiT1.1-N, available from the NanoBiT Multiple Cloning Site Starter System (N2014, Promega Corporation), was cut using SacII and SgfI. HiBiT-NRP1 (WT), HiBiT-NRP1 (Y297A), HiBiT-VEGFR2, SmBiT-NRP1 (WT), SmBiT-NRP1 (Y297A) and SmBiT-VEGFR2 were also cloned in a pFN21A vector with the IL-6 signal peptide, 11 amino acid sequence and a GSSGGSSGAIA linker. The VEGF-A binding-dead mutant of NRP1 (Y297A) was described previously (Peach et al., 2018a). The 11 amino acid NanoBiT tags (HiBiT: VSGWRLFKKIS; SmBIT VTGYRLFEEIL) were obtained as custom oligonucleotide sequences from Sigma-Aldrich, annealed into double stranded DNA and phosphorylated with T4 PNK (New England Biolabs) and inserted using SacII and SgfI sites.

NFAT Luciferase Reporter Gene Assay

HEK293T-NFAT-ReLuc2P cells stably expressed LgBiT-VEGFR2, HiBiT-VEGFR2 or SmBiT-VEGFR2. Cells were seeded at 25,000 cells/well in white 96-well plates pre-coated with poly-D-lysine in DMEM containing 10% FBS. Following incubation for 24 hours at 37%/5% CO2, medium was replaced with serum-free DMEM and cells were incubated for a further 24 hours. On the day of experimentation, medium was replaced with serum-free DMEM containing 0.1% BSA. Cells were stimulated with increasing concentrations of VEGF165a (R&D Systems) for 5 hours at 37%/5% CO2. Medium was replaced with 50 µl/well serum-free DMEM/0.1% BSA and 50 µl/well ONE-Glo Luciferase reagent. Following a 5 minute delay to allow reagent to react with luciferase and background luminescence to subside, luminescence emissions were measured using a TopCount platereader (Perkin Elmer, UK).

Confocal Imaging of HaloTag-VEGFR2 and SnapTag-NRP1

HEK293T-NFAT-ReLuc2P cells were plated in 8-well plates (Nunc Lab-Tek, Thermo Fisher Scientific) pre-coated with poly-D-lysine (0.01mg/ml in PBS) at 30,000 cells per well in DMEM/10% FBS. Following incubation for 24 hours, cells were transfected with a mixture of HaloTag-VEGFR2 and SnapTag-NRP1. Control wells were also transfected with a single construct and empty vector, such as SnapTag-NRP1 and pcDNA3.1/Neo. Transient transfections used FuGENE® HD at a 3:1 ratio of reagent to cDNA with a total 100 ng cDNA/well, with receptors transfected at equal amounts of 50 ng cDNA/well. Transfection solutions were made up in serum-free DMEM and added as 11 µl/well. Cells were incubated for a further 24 hours at 37°C/5% CO2. Receptors were then labelled with a solution of serum-free DMEM/0.1% BSA containing both 0.5 µM membrane impermeant HaloTag-AlexaFluor488 substrate (G1002; Promega Corporation, USA) and 0.5 µM membrane impermeant SNAP-Surface AlexaFluor647 (S9136S; New England BioLabs). These were incubated for 30 minutes (37°C/5% CO2). Cells were washed twice with 200 µl/well HBSS/0.1% BSA, then replaced with a final volume of 225 µl/well. Cells were incubated with vehicle, 10 nM unlabelled VEGF165b or 10 nM unlabelled VEGF165a for 60 minutes at 37°C, adding 25 µl to a total volume of 250 µl. Cells were imaged live using a temperature-controlled LSM710 confocal microscope fit with a 40x water objective (Pan Apochromat objective, NA 1.2). Wavelengths were imaged simultaneously using the 488/561/633 beamsplitter. HaloTag-VEGFR2 AlexaFluor488 was imaged using an Argon 488 nm laser (493-628 nm bandpass; 2.5% power); SnapTag-NRP1 AlexaFluor647 was imaged with a HeNe633 nm laser (638-747 nm; 2.5% power). All images were taken as 12 bit images with 1024x1024 pixels per frame with 4 averages and similar gains per replicate.

Bioluminescence Imaging of NanoBiT Complexes

HEK293T-NFAT-ReLuc2P cells were plated in 6-well plates at 400,000 cells/well in DMEM/10% FBS. On day 2, cells were transfected using FuGENE® HD at a 3:1 ratio of reagent to cDNA with a total 1500 ng cDNA/well made up in serum-free DMEM. Cells were transfected with equal amounts of LgBiT-VEGFR2 (750 ng cDNA/well) and HiBiT-NRP1 WT (750 ng cDNA/well). Alternatively, NanoLuc-VEGFR2 or NanoLuc-NRP1 were transfected at 750 ng cDNA/well with an equal amount of pcDNA3.1/Zeo (750 ng cDNA/well). On day 3, transfected cells were transferred to a 4- compartment 35/10 mm glass bottomed dish (CELLview, Greiner Bio-One). Dishes were pre-coated with poly-D-lysine (0.01mg/ml in PBS) and cells were plated at 75,000 cells/well in DMEM containing 0.1% FBS. On the day of experimentation (day 4), medium was replaced with HBSS/0.1% BSA. For cells expressing full-length NanoLuc, furimazine was added at 26 µM. In contrast, cells expressing the NanoBiT complex were incubated with a higher furimazine concentration (104 µM) for optimal imaging. Following incubation for 10 minutes to allow for substrate oxidation, cells were imaged live at 37°C using the inverted Olympus LV200 Bioluminescence Imaging System, fitted with a 60x oil immersion objective (super Apochromat UPLSAPO 60xO objective; NA 1.35) with a 0.5x tube lens to focus the image, therefore images had a final magnification of 30x. Luminescence was collected using a Hammamatsu Image EMx2 Electron Multiplying Charge Coupled Device (EMCCD) camera. Transmitted light images were collected using the camera in conventional CCD mode with a 200 ms exposure time. Luminescence emissions from the full-length NanoLuc or the NanoBiT complex were measured for 5 second exposure with a gain of 200. Images were taken as 8 bit images with 512x512 pixels per frame.

BRET Between NanoLuc-VEGFR2 and Fluorescent NRP1

HEK293T-NFAT-ReLuc2P cells were plated in white 96-well plates pre-coated with poly-D-lysine (0.01mg/ml in PBS) at 25,000 cells per well in DMEM containing 10% FBS. Following 24 hours, cells were transiently transfected with a total 125 ng cDNA/well using FuGENE® HD at a 3:1 ratio of reagent to cDNA. Cells were transfected with a constant amount of NanoLuc-VEGFR2 (25 ng cDNA/well). Cells were simultaneously transfected with increasing concentrations of HaloTag-NRP1 or SnapTag-NRP1 (2.5-100 ng cDNA/well). Additional wells only contained NanoLuc-VEGFR2. These transfection solutions were made up to equivalent to 125 ng per well using empty pcDNA3.1/Zeo vector in serum-free DMEM. Cells were incubated for

another 24 hours at 37°C/5% CO2. On the day of the experiment, cells were treated with 0.2 μM membrane impermeant HaloTag-AlexaFluor488 substrate or 0.2 μM SNAP-Surface AlexaFluor488 substrate in serum-free-DMEM/0.1% BSA. Cells were incubated for 30 minutes at 37°C/5% CO2. They were then washed twice with 100 μl/well HBSS/0.1% BSA and replaced with a final volume of 50 μl/well HBSS/0.1% BSA. At this stage, fluorescence emissions were quantified using the PHERAstar FS platereader using filters for excitation at 485 nm and emission at 520 nm. Cells were then incubated with the NanoLuc substrate furimazine (10 μM) for 5 minutes. Emissions were recorded using the PHERAstar FS platereader using filters simultaneously measuring NanoLuc emissions at 475 nm (30 nm bandpass) and AlexaFluor488 emissions at 535 nm (30 nm bandpass). BRET ratios were calculated as fluorescence over luminescence emissions from the second of three cycles.

Luminescence from NanoBiT Complementation

To characterise luminescence emissions from a NanoBiT complex, HEK293T-NFAT-ReLuc2P cells were plated as 25,000 cells/well in white 96-well plates pre-coated with poly-D-lysine (0.01mg/ml in PBS) in DMEM containing 10% FBS. Following 24 hours, cells were transiently transfected using FuGENE® HD at a 3:1 ratio of reagent to cDNA with a total 100 ng cDNA/well. Cells were transfected with a combination of LgBiT-tagged (50 ng cDNA/well) and HiBiT-/SmBiT-tagged receptors (50 ng cDNA/well). Alternatively, cells were transfected with single constructs (50 ng cDNA/well) with empty pcDNA3.1/Zeo vector (50 ng cDNA/well). Transfection mixtures were made up in serum-free DMEM and added as 5 μl/well without replacing DMEM/10% FBS on cells. Cells were incubated at 37°C/5% CO2 for a further 24 hours. Medium was replaced with HBSS/0.1% BSA containing 10 μM furimazine, in the absence or presence of purified LgBiT protein (N401B, Promega Corporation) or HiBiT protein (N301A, Promega Corporation). Cells were incubated at 37°C for 10 minutes to allow NanoBiT complementation and the oxidation of furimazine. To prevent the loss of signal through the bottom of the plate, an adhesive plate BackSeal was added at this point. Luminescence emissions were measured on the PHERAstar platereader using the filter settings measuring emissions between 475-505 nm.

Additional experiments aimed to disrupt the recomplemented NanoBiT complex using increasing concentrations of competing receptor. HEK293T-NFAT-ReLuc2P cells were plated as 25,000 cells/well in white 96-well plates pre-coated with poly-D-lysine (0.01mg/ml in PBS) in DMEM containing 10% FBS. Following 24 hours, cells were transiently transfected using FuGENE® HD at a 3:1 ratio of reagent to cDNA. Cells were transfected with a constant amount of LgBiT-VEGFR2 (50 ng cDNA/well) and either HiBiT-NRP1 or SmBiT-NRP1 (50 ng cDNA/well). Cells were also transfected with increasing concentrations of HaloTag-NRP1 (25-200 ng cDNA/well). This was made up to 300 ng cDNA/well with empty pcDNA3.1/Zeo vector. Additional wells only contained the LgBiT-VEGFR2 and HiBiT/SmBiT-NRP1 complex. Cells were incubated with transfection solution for 24 hours at 37°C/5% CO2. On the day of the experiment, cells were treated with 0.2 μM membrane impermeant HaloTag-AlexaFluor488 substrate in serum-free-DMEM/0.1% BSA (30 minutes, 37°C/5% CO2). They were then washed twice with 100 μl/well HBSS/0.1% BSA and replaced with a final volume of 50 μl/well HBSS/0.1% BSA. Fluorescence emissions were quantified using the PHERAstar FS platereader using filters for excitation at 485 nm and emission at 520 nm. Cells were incubated with 10 μM furimazine for 10 minutes, then luminescence and fluorescence emissions were recorded using PHERAstar FS platereader. Emissions were simultaneously measured for NanoLuc at 475 nm (30 nm bandpass) and AlexaFluor488 at 535 nm (30 nm bandpass).

Fluorescent VEGF-A Binding at a VEGFR2/NRP1 NanoBiT Complex

HEK293T-NFAT-ReLuc2P cells were plated in 6-well plates at 400,000 cells/well in DMEM containing 10% FBS. On day 2, cells were transfected using FuGENE® HD at a 3:1 ratio of reagent to cDNA with a total 1500 ng cDNA/well made up in serum-free DMEM. Cells were transfected with equal amounts of LgBiT-VEGFR2 (750 ng cDNA/well) and HiBiT-NRP1 WT or Y297A (750 ng cDNA/well), or equal amounts of LgBiT-VEGFR2 (750 ng cDNA/well) with SmBiT-NRP1 WT (750 ng cDNA/well). For experiments

monitoring kinetics at HiBiT complexes, matched controls were performed alongside in which cells were transfected with single receptors conjugated to full-length NanoLuc. NanoLuc-VEGFR2 or NanoLuc-NRP1 were transfected at 750 ng cDNA/well, made up to 1500 ng cDNA/well with empty pcDNA3.1/Zeo vector (750 ng cDNA/well). On day 3, cells were transferred from 6-well plates. Cells were washed with 1 ml/well PBS, detached with 500 µl/well trypsin and resuspended in 2 ml DMEM containing 10% FBS. Cells were seeded in white 96-well plates pre-coated with poly-D-lysine (0.01mg/ml in PBS) at 30,000 cells/well. On the day of experimentation (day 4), medium was replaced with HBSS/0.1% BSA.

For saturation experiments, increasing concentrations of VEGF165a–TMR or VEGF165b-TMR (0.5-20 nM) were added in the presence or absence of a high concentration of corresponding unlabelled ligand (100nM, ˜100-fold greater than the estimated Kd value). Following incubation for 60 minutes in the dark at 37°C, the NanoLuc substrate furimazine (10 µM) was added to each well and equilibrated for 5 minutes to enable NanoLuc-mediated furimazine oxidation and resulting luminescence emissions. Emissions were recorded using the PHERAstar FS platereader (BMG Labtech) using a filter simultaneously measuring NanoLuc emissions at 450 nm (30 nm bandpass) and TMR emissions using a longpass filter at 550 nm. BRET ratios were calculated as fluorescence over luminescence emissions from the second of three cycles.

For kinetic experiments, cells were pre-treated with furimazine (10 µM) for 5 minutes to enable NanoLuc-mediated furimazine oxidation and resulting luminescence emissions. BRET ratios were then measured per well using the PHERAstar FS platereader using the filters above. Following 4 initial measurements, intact cells were stimulated with 0.5-20 nM VEGF165a-TMR or VEGF165b-TMR Emissions were recorded every 30 seconds for 20 minutes or 90 minutes, using the temperature control function of the PHERAstar FS platereader to maintain conditions at 37°C.

Data Analysis

Data were analysed using GraphPad Prism 7.02 (GraphPad Software, La Jolla, CA, USA). Data are presented as mean ± S.E.M.. Statistical significance was defined as $P< 0.05$. Confocal images were collected using Zen 2010 software (Zeiss, Germany). Confocal images were processed and analysed using ImageJ Fiji 1.52 software (National Institutes of Health, US).

For colocalization analysis, confocal images were corrected to the background fluorescence intensity from each experimental replicate determined using un-transfected cells in each field of view (HaloTag-VEGFR2, 488 nm; SnapTag-NRP1, 647 nm). The mean background intensity was calculated for each experimental replicate (n=4) and subtracted from each image for manual thresholding. To quantify colocalization, regions of interest (ROIs) were drawn around each cell that co-expressed HaloTag-VEGFR2 and SnapTag-NRP1. Following subtraction of the region outside the ROI, colocalisation was determined using pixel-based measures between HaloTag-VEGFR2 and SnapTag-NRP1 using the ImageJ plugin Coloc 2. Mander's Overlap Coefficients measure co-occurrence as the proportion of SnapTag-NRP1 pixels (red) overlapping with HaloTag-VEGFR2 (green). Pearson's Correlation Coefficients measure whether there is a correlation between these channels. Colocalisation parameters were calculated on a per cell basis, with a total number of 97 cells (vehicle) and 54 cells (VEGF165a stimulation) and 68 cells (VEGF165b stimulation), pooled from 4 independent experiments.

Saturation binding curves were fitted simultaneously for total ($VEGF_{165}$a-TMR or $VEGF_{165}$b-TMR alone) and non-specific binding (obtained in the presence of 100 nM of unlabelled VEGF-A) using the equation:

$$Total\ Binding = \ B_{\max}.\frac{[L]}{[L] + \ K_d} + M.[L] + C$$

describing the nanomolar fluorescent ligand concentration, [L]; maximal binding, Bmax; the equilibrium dissociation constant of the labelled ligand, Kd, in the same units as [L], the slope of the non-specific binding component, M; and the y axis intercept, c.

Kinetic studies of fluorescent ligand binding measured over time were fitted to a mono-exponential association function:

$$Binding = y_{\max} \,.\, (1 \; - e^{-k_{\text{obs}} \,\cdot\, \text{t}})$$

describing time, t, plotted on the x axis; maximum response at infinite time, y_{max}; and the rate constant observed for association, k_{obs}. Additionally, k_{on} and k_{off} values were determined by simultaneously fitting association curves at different fluorescent ligand concentrations ([L]). This utilised the following relationship with k_{obs}:

$$k_{\text{obs}} = k_{\text{on}}.\,[L] + \; k_{\text{off}}$$

further describing association rate, k_{on}, in units of min^{-1} M^{-1}; and dissociation rate, k_{off}, in min^{-1}. These kinetic data were also used to estimate the binding affinities, due to the relationship between dissociation and association rates within an equilibrium:

$$K_d = \; \frac{k_{\text{off}}}{k_{\text{on}}}$$

Residence time was calculated as the reciprocal of k_{off}. Additionally, assuming a first order reaction, half life ($t_{1/2}$) was calculated for a given concentration.

$$t_{1/2} = \; \frac{\ln 2}{k_{\text{on}}.\,[L] + \; k_{\text{off}}}$$

$$t_{1/2} = \; \frac{0.693}{k_{\text{obs}}}$$

RESULTS

Co-localisation between VEGFR2 and NRP1 co-expressed in living HEK293T cells

To investigate where VEGFR2 and NRP1 were localised when both receptors were expressed together in HEK293T cells at 37°C, we labelled each cell surface receptor with a distinct fluorophore. Receptors were simultaneously labelled using different substrates containing a HaloTag chloroalkane or SnapTag benzylguanine moiety, exploiting the fact that the membrane-impermeant fluorophore-conjugated substrate only labels receptors at the plasma membrane. HaloTag-VEGFR2 and SnapTag-NRP1 were labelled with membrane-impermeant HaloTag-AlexaFluor488 and SnapTag-AlexaFluor647 (Figure 1a). Constitutive internalisation of HaloTag-VEGFR2 was observed (Figure 1a, green regions) whereas SnapTag-NRP1 was largely expressed at the plasma membrane (Figure 1a, magenta regions). Sites of spatial overlay between VEGFR2 and NRP1 were both intracellular and at regions around the plasma membrane (Figure 1a, white). The same cell population was stimulated with a saturating concentration of unlabelled $VEGF_{165}$b (upper panels) or $VEGF_{165}$a (lower panels) for 60 minutes (Figure 1a, right panels). Representative images show a large proportion of NRP1 remained at the plasma membrane independent of VEGF-A stimulation. To account for heterogeneity between cells, regions of interest were drawn around any cell successfully co-expressing both RTK and co-receptor to quantify colocalisation between HaloTag-VEGFR2 and SnapTag-NRP1. Upon stimulation with VEGFR2-selective $VEGF_{165}$b, there was a reduction in the proportion of NRP1 in VEGFR2-positive regions relative to vehicle (Figure 1b). In contrast, there was a higher correlation between VEGFR2/NRP1

colocalisation upon $VEGF_{165}$a stimulation compared to vehicle (Figure 1c). Both parameters indicated that VEGFR2 and NRP1 were co-localised in the absence of ligand.

BRET can also be applied to monitor proximity between receptors tagged with a bioluminescent donor (NanoLuc) and fluorescent acceptor (AlexaFluor488). Receptor-receptor BRET was used to monitor whether VEGFR2 and NRP1 were in close proximity (<10 nm) when co-expressed in HEK293T cells. This unbiased technique monitors proximity from a whole cell population in 96-well plates. Cells were simultaneously transfected with a constant amount of bioluminescent donor, NanoLuc-VEGFR2, and increasing amounts of cell surface fluorophore-labelled NRP1. In the absence of ligand, there was clear saturation of the BRET signal with increasing amounts of fluorescent NRP1 acceptor (Figure 2a). This was observed for both SnapTag-NRP1 and HaloTag-NRP1, therefore independent of the fluorophore labelling approach. Confirming that increasing amounts of HaloTag-NRP1 and SnapTag-NRP1 were successfully transfected, there was also a saturable BRET signal when plotted against raw fluorescence emissions (Figure 2b). Both techniques confirmed the constitutive formation of heteromeric complexes between VEGFR2 and NRP1 in living cells.

Complementation of NanoBiT fragments using N-terminal tagged VEGFR2 and NRP1

We then applied a split NanoBiT approach to isolate luminescence emissions from a defined VEGFR2/NRP1 heteromeric complex. Enzymatic luciferase activity requires complementation between the large fragment (LgBiT) and the short 11 amino acid tag (HiBiT or SmBiT). To determine the optimal configuration for luminescence emissions, each NanoBiT fragment was appended to the N-terminus of both full-length VEGFR2 or NRP1. Luminescence emissions were higher for the combination with LgBiT-tagged VEGFR2 and the short fragment attached to NRP1 (Figure 3a). Emissions from the HiBiT complex were approximately ten-fold higher than the SmBiT complex. NanoBiT-tagged receptors expressed independently emitted minimal luminescence in the presence of furimazine relative to the complemented NanoBiT complex (Figure 3b). Addition of purified NanoBiT fragments to exogenously complement the NanoBiT tag confirmed that individual constructs were appropriately expressed despite low luminescence emissions in isolation (Figure 3c). The luminescence signals from both HiBiT and SmBiT complexes were also prevented by competition with increasing amounts of unlabelled HaloTag NRP1 (Figure 3d). Thus, despite the intrinsic affinity between HiBiT and LgBiT (Dixon et al., 2016), luminescence emissions were reduced by increasing amounts of NRP1.

A bioluminescence widefield imaging system was used to visualise where the NanoBiT luminescence signal was localised. To determine the cellular location of the NanoBiT complexes, cells were incubated with membrane-permeable furimazine in the absence of ligand (Figure 4). The NanoBiT complex between HiBiT-NRP1 and LgBiT-VEGFR2 was localised to both intracellular sites and the plasma membrane. This spatial distribution was comparable to the regions of white overlay between HaloTag-VEGFR2 and SnapTag-NRP1 observed in Figure 1a.

Influence of NanoBiT tags on VEGFR2-mediated signalling.

We confirmed that the NanoBiT fragments did not interfere with VEGFR2 signalling using an NFAT reporter gene assay (Kilpatrick et al., 2017). Concentration-response curves for $VEGF_{165}$a were compared between cells stably expressing VEGFR2 tagged at the N-terminus with LgBiT, HiBiT or SmBiT (Figure 5). Each receptor exhibited a concentration-dependent increase in NFAT gene transcription in response to increasing concentrations of VEGF165a. Each cell line had a similar potency derived for $VEGF_{165}$a (LgBiT-VEGFR2 $pEC_{50} = 9.95 \pm 0.11$; HiBiT-VEGFR2 $pEC_{50} = 10.06 \pm 0.12$; SmBiT-VEGFR2 $pEC_{50} = 10.23 \pm 0.23$; n=5 for each). These were comparable to potency values derived for $VEGF_{165}$a at wild type VEGFR2 (Kilpatrick et al., 2017).

Nanomolar affinity of fluorescent VEGF-A at a defined VEGFR2/NRP1 complex

Fluorescent VEGF-A ligand binding was monitored at full-length VEGFR2 and NRP1 tagged at their N-terminus with LgBiT and HiBiT, respectively. Since uncomplemented receptors cannot oxidise furimazine, luminescence was confined to proteins where complementation from a defined heteromeric VEGFR2/NRP1 NanoBiT complex had occurred (Figure 6a). BRET therefore only derived from the receptor/co-receptor complex and the fluorescent VEGF-A acceptor. We have previously demonstrated that $VEGF_{165}$b-TMR selectively binds to NanoLuc-VEGFR2 (and not NRP1), whereas $VEGF_{165}$a-TMR can bind to both NanoLuc-VEGFR2 or NanoLuc-NRP1 with nanomolar affinity (Peach et al., 2018a). At the complemented HiBiT complex, there was saturable binding in the presence of increasing concentrations of $VEGF_{165}$b-TMR (Figure 6b) or $VEGF_{165}$a-TMR (Figure 6c). This was displaced by a high concentration of unlabelled ligand, demonstrating low non-specific binding. Both fluorescent ligands had equilibrium dissociation constants (K_d) in the nanomolar range at the VEGFR2/NRP1 complex ($VEGF_{165}$b-TMR $K_d = 16.26 \pm 3.81$ nM, $pK_d = 7.82 \pm 0.11$; $VEGF_{165}$a-TMR $K_d = 2.53 \pm 0.49$, $pK_d = 8.61 \pm 0.09$; n=3 for both). Estimated ligand binding affinities were similar to those derived at isolated receptors tagged with full-length NanoLuc (Peach et al., 2018a).

Real-time kinetics of fluorescent VEGF-A isoforms at a heteromeric VEGFR2/NRP1 NanoBiT complex

Taking advantage of the NanoBiT approach to monitor real-time ligand binding at 37°C to a complex, we compared the kinetics of ligand binding of $VEGF_{165}$b-TMR with that of $VEGF_{165}$a-TMR at the VEGFR2/NRP1 NanoBiT complex in living cells. The kinetic binding profile of $VEGF_{165}$b-TMR (which should only bind to VEGFR2; Peach et al., 2018a) continued to increase over the full 90 minute time course in intact cells, producing a classic ligand binding association maintained for each concentration of $VEGF_{165}$b-TMR (Figure 7a). Fitted to a global association curve (Table 1), $VEGF_{165}$b-TMR had a slightly slower association rate constant (k_{on}) for the VEGFR2/NRP1 complex ($2.29 \times 10^6 \pm 0.30 \times 10^6 min^{-1}.M^{-1}$) compared to NanoLuc-VEGFR2 alone ($7.29 \times 10^6 min^{-1}.M^{-1}$; Peach et al., 2018a). We then directly compared the real-time binding profile for a saturating concentration of $VEGF_{165}$b-TMR between the NanoBiT complex and cells expressing NanoLuc-tagged receptors alone in matched time course experiments (Figure 7b). Compared to NanoLuc-VEGFR2, the small decline in BRET signal after a peak at 20 minutes in intact cells was absent when monitored at the NanoBiT complex for $VEGF_{165}$b-TMR. There was no BRET detected between $VEGF_{165}$b-TMR and NanoLuc-NRP1, however this selective ligand had a distinct long-term kinetic profile at the VEGFR2/NRP1 complex compared to VEGFR2 alone (Figure 7b).

Kinetic experiments were repeated with four concentrations of $VEGF_{165}$a-TMR (Figure 7c). Unlike $VEGF_{165}$b-TMR, there was a small decline in BRET ratio between 30-60 minutes for $VEGF_{165}$a-TMR at the HiBiT complex (Figure 7c). Association binding curves were globally fitted to kinetic data from the initial 20 minutes due to this decline (Table 1). $VEGF_{165}$a-TMR had a slower dissociation rate constant (k_{off}) at the HiBiT complex (0.046 ± 0.007 min^{-1}; Table 1) compared to that previously reported for NanoLuc-NRP1 expressed alone (0.26 min^{-1}; Peach et al., 2018a). As a consequence, the kinetic binding profile for 10 nM $VEGF_{165}$a-TMR was directly compared between the NanoBiT complex and either NanoLuc-VEGFR2 or NanoLuc-NRP1 (Figure 7d). $VEGF_{165}$a-TMR association kinetics at the NanoBiT complex in the initial 20 minutes were more comparable to NanoLuc-VEGFR2 than NanoLuc-NRP1 (NanoBiT $k_{obs} = 0.33 \pm 0.04$ min^{-1}, NanoLuc-VEGFR2 $k_{obs} = 0.31 \pm 0.03$ min^{-1}, NanoLuc-NRP1 $k_{obs} = 0.93 \pm 0.09$ min^{-1}; n=5 per group). These observed rate constants were significantly slower at the complex than NRP1 alone (repeated-measures ANOVA and Holm-Šidák's multiple comparisons;$P< 0.05$, n=5 for each). These data suggest that the ligand binding profile for $VEGF_{165}$a-TMR at the NanoBiT complex reflected VEGFR2 binding kinetics, as opposed to the faster binding observed at NRP1.

Fluorescent VEGF-A kinetics were similar for the SmBiT Complex

Considering the distinct kinetic observations at the HiBiT complex, we further probed ligand binding kinetics at the SmBiT complex to explore possible influences of the NanoBiT tag characteristics (Dixon et al., 2016). Using four concentrations of $VEGF_{165}$b-TMR, binding was monitored over 90 minutes (Figure 8a). The binding profile remained elevated throughout the time course with similarities to kinetics observed with the HiBiT complex. Kinetic data were globally fitted to a simple exponential association (Table 1). $VEGF_{165}$b-TMR had a slower dissociation rate (k_{off}) from the SmBiT complex compared to the HiBiT complex (Kruskal-Wallis test, $P< 0.05$, n=5 per group). Plotting the individual observed association rate constants (k_{obs}) against $VEGF_{165}$b-TMR concentration, there was a linear relationship observed at both HiBiT and SmBiT complexes (Figure 8b). The interaction between $VEGF_{165}$b-TMR and the NanoBiT complex can therefore be defined as a first order reaction. Binding kinetics were also monitored at the SmBiT complex using four concentrations of $VEGF_{165}$a-TMR (Figure 8c). Fitted data from the initial 20 minute period using a global fit, there were no differences between the association kinetic parameters derived for $VEGF_{165}$a-TMR for the HiBiT and SmBiT complexes (Kruskal-Wallis test and Dunn's multiple comparisons test,$P> 0.05$, n=5 per group). There was a linear relationship between the derived observed association rate (k_{obs}) constants and $VEGF_{165}$a-TMR concentration (Figure 8d). Despite having the potential to bind to both receptors within the complex, the interaction between $VEGF_{165}$a-TMR and the NanoBiT complex could also be defined by a first order reaction.

Similar complex pharmacology using a binding-dead mutant of NRP1

In addition to comparing binding between selective and non-selective fluorescent VEGF-A isoforms, site-directed mutagenesis was an alternative approach to probe the contribution of NRP1 engagement to the pharmacological characteristics of the VEGFR2/NRP1 complex. Using a previously characterised binding-dead NRP1 mutant (Y297A; Herzog et al., 2011; Fantin et al., 2014; Peach et al., 2018a), comparisons were made using the same ligand in the absence of interactions between $VEGF_{165}$a-TMR and NRP1 within the heteromeric NanoBiT complex (Figure 9a). Upon co-expression of LgBiT-VEGFR2 and either HiBiT- or SmBiT-NRP1 (Y297A), there were high luminescence emissions resulting from NanoBiT complementation (Figure 9b). Luminescence emissions from this NanoBiT complex were comparable to wild type NRP1, therefore this amino acid residue was not required for constitutive VEGFR2/NRP1 complex formation. NanoBiT constructs expressed in isolation from their complementary fragment also had minimal luminescence emissions in the presence of furimazine (Figure 9b). Isolating ligand binding from this VEGFR2/NRP1 Y297A complex, $VEGF_{165}$a-TMR exhibited saturable binding at the NanoBiT complex (Figure 9c). This was displaced by a high concentration of unlabelled $VEGF_{165}$a, confirming that there was low non-specific binding. Derived equilibrium dissociation constants were in the nanomolar range and similar to the wild type NanoBiT complex ($VEGF_{165}$a-TMR/NanoBiT Y297A K_d = 1.55 ± 0.38; pK_d 8.84 ± 0.11; n=3). Binding kinetics at the mutant NanoBiT complex were then monitored using four concentrations of $VEGF_{165}$a-TMR (Figure 9d). This had an identical profile compared to $VEGF_{165}$a-TMR at the wild type HiBiT complex (Figure 7c), whereby there was a small decline in BRET ratio following 30-60 minutes. Association kinetics were derived from the initial 20 minutes using a global fit (k_{on} = $3.71x10^7$ ± $0.21x10^7 min^{-1}M^{-1}$; k_{off} = 0.054 ± 0.008 min^{-1}; kinetic pK_d = 8.85 ± 0.04; n=5). These data suggest that $VEGF_{165}$a-TMR bound the NanoBiT complex with similar kinetics, regardless of the ability to simultaneously engage NRP1.

DISCUSSION

NanoBiT technologies were used to quantify the real-time binding of two fluorescent VEGF-A isoforms at a defined receptor/co-receptor complex between VEGFR2 and NRP1 in living cells at 37°C. Previous work identified differences between VEGFR2 and NRP1 pharmacology in terms of their binding kinetics and localisation when expressed on their own (Peach et al., 2018a). VEGFR2 and NRP1 are, however, endogenously co-expressed together in endothelial cells and tumour cells (Whitaker et al., 2001; Prahst

et al., 2008; Fantin et al., 2013; Koch et al., 2014; Lee-Montiel et al., 2015). We first demonstrated that full-length VEGFR2 and NRP1 constitutively formed a heteromeric complex in living HEK293T cells. To then probe how this specific receptor/co-receptor heteromer interacted with ligand, we established a novel approach to quantify fluorescent VEGF-A binding at a defined complex using split NanoBiT fragments (Dixon et al., 2016). VEGFR2 and NRP1 tagged at their N-terminus with HiBiT and LgBiT tags led to NanoBiT complementation with minimal luminescence when each was expressed alone. The formation of this NanoBiT complex could be prevented by increasing amounts of an unlabelled version of one of the heteromer components. As such, the BRET signal was specific to interactions between the VEGFR2/NRP1 heteromer (BRET donor) and fluorescent VEGF-A (BRET acceptor). This allowed us to monitor ligand binding to a defined RTK/co-receptor oligomeric complex. Un-complemented VEGFR2 or NRP1 that still bind to the fluorescent ligand do not, however, contribute to the BRET signal due to the lack of complemented donor luminescence and the requirement for donor and acceptor to be within 10 nm of each other.

Numerous biochemical techniques have suggested that VEGFR2 and NRP1 form heteromeric complexes, including co-immunoprecipitation studies in endothelial cells (Whitaker et al., 2001; Prahst et al., 2008; Gelfand et al., 2014) and proximity-ligation assays using antibodies *in situ* on tumour tissue (Koch et al., 2014). Förster Resonance Energy Transfer has also been used to demonstrate complex formation using truncated VEGFR2 and full-length NRP1 tagged with fluorophores at their C-terminus (King et al., 2018). Here, we initially used BRET between full-length VEGFR2 and NRP1 tagged at their N-terminus with NanoLuc or a fluorophore to confirm complex formation in the absence of added VEGF-A. The approach monitored complex formation that originated at the cell membrane since membrane-impermeant fluorophore-conjugated HaloTag or SnapTag substrates were used. Basal VEGFR2/NRP1 complex formation was also confirmed using both HiBiT-VEGFR2 and LgBiT-NRP1 complementation and the reverse LgBiT-VEGFR2 and HiBiT-NRP1 orientation.

Following the discovery that $VEGF_{165}$a had faster binding kinetics for binding to NRP1 than to VEGFR2 when expressed on their own (Peach et al., 2018a), it was proposed that the presence of NRP1 might enhance $VEGF_{165}$a binding to the heteromeric complex. The application of both NanoBiT technology and NanoBRET to monitor exclusively $VEGF_{165}$a-TMR binding to VEGFR2/NRP1 complexes allowed us to test this hypothesis directly. Interestingly, the initial association kinetics (during the first 20 minutes) for $VEGF_{165}$a-TMR binding to the VEGFR2/NRP1 heteromeric complex were closer to those observed at NanoLuc-VEGFR2 in isolation than to NanoLuc-NRP1. This was evident from quantification of the observed rate constant from matched experiments at a saturating concentration (10 nM) of fluorescent $VEGF_{165}$a where k_{obs} was 0.33 ± 0.04 min^{-1} for the VEGFR2/NRP1 NanoBit complex, 0.31 ± 0.03 min^{-1} for NanoLuc-VEGFR2 and 0.93 ± 0.09 min^{-1} for NanoLuc-NRP1. Furthermore, the removal of the binding site for $VEGF_{165}$a on NRP1 by site-directed mutagenesis of residue Y297 to alanine did not alter the ability of VEGFR2 and NRP1 to form complexes or the binding of $VEGF_{165}$a-TMR to the heteromeric complex. It is possible therefore that heteromerization between VEGFR2 and NRP1 masks the high affinity binding site for $VEGF_{165}$a on NRP1 and just leaves the VEGFR2 binding site available.

There were some subtle differences between the kinetics of fluorescent VEGF-A isoforms at the VEGFR2/NRP1 heteromeric complex. Pro-angiogenic $VEGF_{165}$a and anti-angiogenic $VEGF_{165}$b are functionally distinct VEGF-A isoforms, however these isoforms only differ by six amino acid residues at their C-terminus. Despite observed physiological distinctions between VEGF-A isoforms, there were no differences observed at the level of ligand binding to NanoLuc-VEGFR2 when it was expressed alone (Peach et al., 2018a). $VEGF_{165}$b is, however, selective for VEGFR2 and unable to interact with NRP1 (Peach et al., 2018a). The real-time BRET signal for $VEGF_{165}$b-TMR remained elevated in intact cells at the NanoBiT complex over the full 90-minute time course. This resembled observations made with NanoLuc-VEGFR2 in membrane preparations and was quite different to the decline in BRET signal normally observed in intact HEK293T cells (Peach et al., 2019). In contrast, the profile for $VEGF_{165}$a-TMR at the HiBiT complex had a small decrease at latter time points, albeit to a lesser extent than at NanoLuc-VEGFR2 in intact cells (Peach et al., 2019). This reduction in BRET signal for NanoLuc-VEGFR2 following 20 minutes has been linked to VEGF-A/VEGFR2 endocytosis leading to a change in localisation and local pH, as this decline

was absent in membrane preparations and not observed for binding to NanoLuc-NRP1 (Peach et al, 2019). These data suggest that the presence of NRP1 in VEGFR2 heteromeric complexes may reduce the extent of VEGFR2 endocytosis normally seen when VEGFR2 is expressed alone.

Imaging studies exploited the compatibility of HaloTag and SnapTag technologies to label distinct receptors co-expressed by the same cell to monitor colocalisation at 37°C. Unlike immunofluorescent antibody labelling, these experiments can be performed in living cells and do not require cell fixation or cell permeabilization to access internalised receptor. These distinct tags confirmed that VEGFR2 was largely intracellular whereas NRP1 was highly localised around the plasma membrane when they were both co-expressed in the same cell. NRP1 was also localised in filopodia-like projections in HEK293T cells that resembled the filopodia of endothelial tip cells (Fantin et al., 2013, 2015). Although co-localisation studies were limited by the axial resolution limit of basic confocal microscopy, experiments monitoring receptor-receptor BRET confirmed that VEGFR2 and NRP1 were in close proximity (<10 nm). Live cell confocal imaging and bioluminescence imaging data both suggested that VEGFR2 and NRP1 were colocalised in both intracellular compartments and at the plasma membrane. VEGFR2 is subject to macropinocytosis in the absence or presence of ligand (Basagiannis and Christoforidis, 2016; Basagiannis et al., 2016). This bulk transport mechanism could therefore non-selectively engulf surrounding NRP1 in living cells. There is evidence in HUVECs for colocalisation between VEGFR2 and NRP1 both at the plasma membrane in the absence of stimulation (Lee-Montiel et al., 2015) or within intracellular sites following 20 minute $VEGF_{165}$a stimulation (Muhl et al., 2017). As the NanoLuc/NanoBiT substrate furimazine is membrane-permeable, luminescence could be emitted from complexes anywhere in the cell regardless of subcellular localisation.

NanoBiT technologies take advantage of NanoLuc, a small enzyme engineered from a deep sea shrimp with bright, ATP-independent luminescence emissions (Hall et al., 2012). The small, 11 amino acid NanoBiT fragment also has mutations that confer differing intrinsic affinities for the LgBiT fragment. For example, HiBiT has a much higher intrinsic affinity for LgBiT than SmBiT (Dixon et al., 2016). Luminescence emissions from HiBiT-containing complexes were higher than for the corresponding SmBiT-containing complex, as observed previously for NanoBiT-tagged GPCRs (Botta et al., 2019). The intrinsic affinity between HiBiT and LgBiT can vary according to the expression system and protein conformation, as observed for chemokine GPCRs using the purified exogenous tag in different assay setups (White et al., 2020). While the intrinsic affinity between NanoBiT tags should be considered, luminescence emissions from both HiBiT and SmBiT complexes were displaceable by increasing amounts of competing NRP1 (Figure 3d). The kinetic parameters derived from HiBiT and SmBiT complexes were also comparable suggesting that VEGFR2-NRP1 complex formation was not being driven by the affinity of the HiBiT tag for LgBiT.

Despite its ability to upregulate VEGF-A/VEGFR2 signalling in physiological and patho-physiology, the mechanism by which NRP1 upregulates VEGFR2 signalling remains largely unknown. NRP1 can interact with a number of other growth factors (West et al., 2005; Banerjee et al., 2006; Rizzolio et al., 2012), therefore understanding how NRP1 co-expression influences RTK function has implications for other receptors contributing to cancer drug resistance. Our NanoBiT approach allowed us to isolate VEGF-A ligand binding at a defined complex of VEGFR2 and NRP1 and suggested that NRP1 did not increase the affinity or association binding kinetics of $VEGF_{165}$a at VEGFR2. While NRP1 appeared to have no direct effect on ligand binding to a VEGFR2/NRP1 complex expressed within the same cell, NRP1 (which is quite often expressed endogenously at higher levels than VEGFR2) could still act as a reservoir for growth factors and create a localised gradient due to its interactions with the extracellular matrix (Shintani et al., 2006; Windwarder et al., 2016).

In summary, we have described here an approach using NanoBiT technology and NanoBRET to monitor in real time the binding of VEGF-A isoforms to defined heteromeric complexes containing both VEGFR2 and NRP1. This allowed us to determine for the first time the ligand-binding kinetics of $VEGF_{165}$a-TMR and $VEGF_{165}$b-TMR to the VEGFR2-NRP1 complex. We were able to use bioluminescence imaging and confocal microscopy to determine that VEGFR2-NRP1 complexes are localised in both intracellular compartments and at the plasma membrane. At the plasma membrane, the presence of NRP1 within the heteromeric com-

plex appeared to reduce the extent of agonist-induced VEGFR2 endocytosis normally observed when it is expressed alone. The presence of NRP1 within the VEGFR2-NRP1 heteromeric complexes did not enhance $VEGF_{165}$a-TMR binding, and a NRP1 binding-dead mutant (Y297A) had no effect on the binding of $VEGF_{165}$a-TMR, or the formation of VEGFR2-NRP1 complexes, suggesting that the high affinity binding site for $VEGF_{165}$a on NRP1 might be masked within the heteromeric complexes. In keeping with this conclusion $VEGF_{165}$b-TMR, which does not bind to NRP1, had a very similar binding profile to the heteromeric complex to that observed with $VEGF_{165}$a-TMR. This approach to monitor the binding profile of defined oligomeric complexes should be applicable to a wide range of receptor systems and facilitate drug discovery aimed a heteromeric complexes.

ACKNOWLEDGEMENTS

This work was funded by BBSRC (grant number BB/L019418/1) and the British Pharmacological Society. CJP held an AJ Clark studentship from the British Pharmacological Society. LEK holds an Anne McLaren Fellowship from the University of Nottingham. We thank the Centre of Membrane Proteins and Receptors (COMPARE) for financial support and Promega Corporation for synthesising $VEGF_{165}$a-TMR and $VEGF_{165}$b-TMR and providing HaloTag- and NanoLuc-tagged constructs. We also thank the School of Life Sciences Imaging (SLIM) team for support in imaging facilities and analysis.

AUTHOR CONTRIBUTIONS

Conceived the study: Hill, Woolard, Kilpatrick, Peach.

Participated in research design: Peach, Kilpatrick, Hill, Woolard.

Conducted experiments: Peach.

Performed data analysis: Peach, Hill.

Wrote or contributed to the writing of the manuscript: Peach, Kilpatrick, Woolard, Hill.

CONFLICT OF INTEREST

The authors declare no conflicts of interest.

REFERENCES

Ballmer-Hofer, K., Andersson, A.E., Ratcliffe, L.E., and Berger, P. (2011). Neuropilin-1 promotes VEGFR-2 trafficking through Rab11 vesicles thereby specifying signal output. *Blood 118* : 816–26.

Banerjee, S., Sengupta, K., Dhar, K., Mehta, S., D'Amore, P., Dhar, G., et al. (2006). Breast Cancer Cells Secreted Platelet-Derived Growth Factor-Induced Motility of Vascular Smooth Muscle Cells Is Mediated Through Neuropilin-1. *Mol. Carcinog. 45* : 871–80.

Basagiannis, D., and Christoforidis, S. (2016). Constitutive endocytosis of VEGFR2 protects the receptor against shedding. *J. Biol. Chem. 291* : 16892–903.

Basagiannis, D., Zografou, S., Murphy, C., Fotsis, T., Morbidelli, L., Ziche, M., et al. (2016). VEGF induces signalling and angiogenesis by directing VEGFR2 internalisation via macropinocytosis. *J. Cell Sci. 129* : 4091–104.

Botta, J., Bibic, L., Killoran, P., McCormick, P., and Howell, L. (2019). Design and development of stapled transmembrane peptides that disrupt the activity of G-protein coupled receptor oligomers. *J. Biol. Chem. 294* : 16587–603.

Brozzo, M.S., Bjelic, S., Kisko, K., Schleier, T., Leppánen, V.-M., Alitalo, K., et al. (2011). Thermodynamic and structural description of allosterically regulated VEGF receptor 2 dimerization. *Blood119* : 1781–88.

Carmeliet, P. (2005). Angiogenesis in life, disease and medicine.*Nature 438* : 932–36.

Cébe Suarez, S., Pieren, M., Cariolato, L., Arn, S., Hoffman, U., Bogucki, A., et al. (2006). A VEGF-A splice variant defective for heparan sulfate and neuropilin-1 binding shows attenuated signaling through VEGFR-2. Cell. Mol. *Life Sci. 63* : 2067–77.

Chung, A.S., and Ferrara, N. (2011). Developmental and pathological angiogenesis. *Annu. Rev. Cell Dev. Biol. 27* : 563–84.

Delcombel, R., Janssen, L., Vassy, R., Gammons, M., Haddad, O., Richard, B., et al. (2013). New prospects in the roles of the C-terminal domains of VEGF-A and their cooperation for ligand binding, cellular signaling and vessels formation. *Angiogenesis 16* : 353–71.

Dixon, A.S., Schwinn, M.K., Hall, M.P., Zimmerman, K., Otto, P., Lubben, T.H., et al. (2016). NanoLuc Complementation Reporter Optimized for Accurate Measurement of Protein Interactions in Cells. *ACS Chem. Biol. 11* : 400–08.

Djordjevic, S., and Driscoll, P.C. (2013). Targeting VEGF signalling via the neuropilin co-receptor. *Drug Discov. Today 18* : 447–45.

Eswarappa, S.M., Potdar, A.A., Koch, W.J., Fan, Y., Vasu, K., Lindner, D., et al. (2014). Programmed translational readthrough generates antiangiogenic VEGF-Ax. *Cell 157* : 1605–18.

Ewan, L.C., Jopling, H.M., Jia, H., Mittar, S., Bagherzadeh, A., Howell, G.J., et al. (2006). Intrinsic tyrosine kinase activity is required for vascular endothelial growth factor receptor 2 ubiquitination, sorting and degradation in endothelial cells. *Traffic 7* : 1270–82.

Fantin, A., Herzog, B., Mahmoud, M., Yamaji, M., Plein, A., Denti, L., et al. (2014). Neuropilin 1 (NRP1) hypomorphism combined with defective VEGF-A binding reveals novel roles for NRP1 in developmental and pathological angiogenesis. *Development 141* : 556–62.

Fantin, A., Lampropoulou, A., Gestri, G., Raimondi, C., Senatore, V., Zachary, I., et al. (2015). NRP1 Regulates CDC42 Activation to Promote Filopodia Formation in Endothelial Tip Cells. *Cell Rep.11* : 1577–90.

Fantin, A., Schwarz, Q., Davidson, K., Normando, E.M., Denti, L., and Ruhrberg, C. (2011). The cytoplasmic domain of neuropilin 1 is dispensable for angiogenesis, but promotes the spatial separation of retinal arteries and veins. *Development 138* : 4185–91.

Fantin, A., Vieira, J.M., Plein, A., Denti, L., Fruttiger, M., Pollard, J.W., et al. (2013). NRP1 acts cell autonomously in endothelium to promote tip cell function during sprouting angiogenesis. *Blood121* : 2352–62.

Gelfand, M. V, Hagan, N., Tata, A., Oh, W.-J., Lacoste, B., Kang, K.-T., et al. (2014). Neuropilin-1 functions as a VEGFR2 co-receptor to guide developmental angiogenesis independent of ligand binding. *eLife3* : e03720. doi: 10.7554/eLife.03720.

Goel, H.L., and Mercurio, A.M. (2013). VEGF targets the tumour cell.*Nat. Rev. Cancer 13* : 871–82.

Hall, M.P., Unch, J., Binkowski, B.F., Valley, M.P., Butler, B.L., Wood, M.G., et al. (2012). Engineered luciferase reporter from a deep sea shrimp utilizing a novel imidazopyrazinone substrate. *ACS Chem. Biol. 7* : 1848–57.

Herzog, B., Pellet-Many, C., Britton, G., Hartzoulakis, B., and Zachary, I.C. (2011). VEGF binding to NRP1 is essential for VEGF stimulation of endothelial cell migration, complex formation between NRP1 and VEGFR2, and signaling via FAK Tyr407 phosphorylation. *Mol. Biol. Cell22* : 2766–76.

Jubb, A.M., Strickland, L.A., Liu, S.D., Mak, J., Schmidt, M., and Koeppen, H. (2012). Neuropilin-1 expression in cancer and development.*J. Pathol. 226* : 50–60.

Kawamura, H., Li, X., Harper, S.J., Bates, D., and Claesson-Welsh, L. (2008). Vascular Endothelial Growth Factor (VEGF)-A165b Is A Weak In vitro Agonist for VEGF Receptor-2 Due to Lack of Coreceptor Binding and Deficient Regulation of Kinase Activity. *Cancer Res. 68* : 4683–92.

Kilpatrick, L.E., Friedman-Ohana, R., Alcobia, D.C., Riching, K., Peach, C.J., Wheal, A., et al. (2017). Real-time analysis of the binding of fluorescent $VEGF_{165}$a to VEGFR2 in living cells: Effect of receptor tyrosine kinase inhibitors and fate of internalized agonist-receptor complexes. *Biochem. Pharmacol. 136* : 62–75.

King, C., Wirth, D., Workman, S., and Hristova, K. (2018). Interactions between NRP1 and VEGFR2 molecules in the plasma membrane. *Biochim. Biophys. Acta - Biomembr. 1860* : 2118–25.

Koch, S., Meeteren, L.A. Van, Morin, E., Testini, C., Weström, S., Björkelund, H., et al. (2014). NRP1 Presented in trans to the endothelium arrests VEGFR2 endocytosis, preventing angiogenic signaling and tumor initiation. *Dev. Cell 28* : 633–46.

Koch, S., Tugues, S., Li, X., Gualandi, L., and Claesson-Welsh, L. (2011). Signal transduction by vascular endothelial growth factor receptors. *Biochem. J. 437* : 169–83.

Lee-Montiel, F.T., Li, P., and Imoukhuede, P.I. (2015). Quantum dot multiplexing for the profiling of cellular receptors. Nanoscale 18504–18514.

Lee, S.W., Lee, J.E., Yoo, C.Y., Ko, M.S., Park, C.S., and Yang, S.H. (2014). NRP-1 expression is strongly associated with the progression of pituitary adenomas. Oncol. Rep. *32* : 1537–1542.

Leppanen, V.M., Prota, A.E., Jeltsch, M., Anisimov, A., Kalkkinen, N., Strandin, T., et al. (2010). Structural determinants of growth factor binding and specificity by VEGF receptor 2. *Proc. Natl. Acad. Sci. U.S.A. 107* : 2425–30.

Mamluk, R., Gechtman, Z., Kutcher, M.E., Gasiunas, N., Gallagher, J., and Klagsbrun, M. (2002). Neuropilin-1 binds vascular endothelial growth factor 165, placenta growth factor-2, and heparin via its b1b2 domain.*J. Biol. Chem. 277* : 24818–25.

Muhl, L., Folestad, E.B., Gladh, H., Wang, Y., Moessinger, C., Jakobsson, L., et al. (2017). Neuropilin 1 binds platelet-derived growth factor (PDGF)-D and is a co-receptor in PDGF-D/PDGF receptor β signaling. *J. Cell Sci. 130* : 1365–78.

Parker, M.W., Xu, P., Li, X., and Vander Kooi, C.W. (2012). Structural basis for selective vascular endothelial growth factor-A (VEGF-A) binding to neuropilin-1. *J. Biol. Chem. 287* : 11082–89.

Peach, C.J., Kilpatrick, L.E., Friedman-Ohana, R., Zimmerman, K., Robers, M.B., Wood, K. V., et al. (2018a). Real-Time Ligand Binding of Fluorescent VEGF-A Isoforms that Discriminate between VEGFR2 and NRP1 in Living Cells. *Cell Chem. Biol. 25* : 1208–18.

Peach, C.J., Mignone, V.W., Arruda, M.A., Hill, S.J., Kilpatrick, L.E., and Woolard, J. (2018b). Molecular Pharmacology of VEGF-A Isoforms: Binding and Signalling at VEGFR2. *Int. J. Mol. Sci. 19* : 1–27.

Peach, C.J., Kilpatrick, L.E., Woolard, J., and Hill, S.J. (2019). Comparison of the ligand binding properties of fluorescent VEGF-A isoforms to VEGFR2 in living cells and membrane preparations using NanoBRET. *Br. J. Pharmacol. 176* : 3220–35.

Prahst, C., Héroult, M., Lanahan, A.A., Uziel, N., Kessler, O., Shraga-Heled, N., et al. (2008). Neuropilin-1-VEGFR-2 complexing requires the PDZ-binding domain of neuropilin-1. *J. Biol. Chem.283* : 25110–14.

Rizzolio, S., Rabinowicz, N., Rainero, E., Lanzetti, L., Serini, G., Norman, J., et al. (2012). Neuropilin-1-dependent regulation of EGF-receptor Signaling. *Cancer Res. 72* : 5801–11.

Roy, S., Bag, A.K., Singh, R.K., Talmadge, J.E., Batra, S.K., and Datta, K. (2017). Multifaceted role of neuropilins in the immune system: Potential targets for immunotherapy. *Front. Immunol. 8* : 1–27.

Ruch, C., Skiniotis, G., Steinmetz, M.O., Walz, T., and Ballmer-Hofer, K. (2007). Structure of a VEGF–VEGF receptor complex determined by electron microscopy. *Nat. Struct. Mol. Biol. 14* : 249–50.

Shintani, Y., Takashima, S., Asano, Y., Kato, H., Liao, Y., Yamazaki, S., et al. (2006). Glycosaminoglycan modification of neuropilin-1 modulates VEGFR2 signaling. *EMBO J. 25* : 3045–55.

Simons, M., Gordon, E., and Claesson-Welsh, L. (2016). Mechanisms and regulation of endothelial VEGF receptor signalling. *Nat. Rev. Mol. Cell Biol. 17* : 611–25.

Soker, S., Miao, H.Q., Nomi, M., Takashima, S., and Klagsbrun, M. (2002). VEGF165 mediates formation of complexes containing VEGFR-2 and neuropilin-1 that enhance VEGF165-receptor binding. *J. Cell. Biochem. 85* : 357–68.

Soker, S., Takashima, S., Hua, Miao, Q., Neufeld, G., and Klagsbrun, M. (1998). Neuropilin-1 Is Expressed by Endothelial and Tumor Cells as an Isoform-Specific Receptor for Vascular Endothelial Growth Factor. *Cell 92* : 735–45.

Stoddart, L., Johnstone, E.K.M., Wheal, A.J., Goulding, J., Robers, M.B., Machleidt, T., et al. (2015). Application of BRET to monitor ligand binding to GPCRs. *Nat. Methods 12* : 661–63.

Stoddart, L.A., Kilpatrick, L.E., and Hill, S.J. (2017). NanoBRET Approaches to Study Ligand Binding to GPCRs and RTKs. Trends Pharmacol. Sci. *39* : 136–47.

Vander Kooi, C.W., Jusino, M.A., Perman, B., Neau, D.B., Bellamy, H.D., and Leahy, D.J. (2007). Structural basis for ligand and heparin binding to neuropilin B domains. *Proc. Natl. Acad. Sci. U.S.A.104* : 6152–57.

Vempati, P., Popel, A.S., and Mac Gabhann, F. (2014). Extracellular regulation of VEGF: Isoforms, proteolysis, and vascular patterning. *Cytokine Growth Factor Rev . 25* : 1–19.

West, D.C., Rees, C.G., Duchesne, L., Patey, S.J., Terry, C.J., Turnbull, J.E., et al. (2005). Interactions of multiple heparin binding growth factors with neuropilin-1 and potentiation of the activity of fibroblast growth factor-2. *J. Biol. Chem. 280* : 13457–64.

Whitaker, G.B., Limberg, B.J., and Rosenbaum, J.S. (2001). Vascular Endothelial Growth Factor Receptor-2 and Neuropilin-1 Form a Receptor Complex that is Responsible for the Differential Signaling Potency of VEGF165 and VEGF121. *J. Biol. Chem. 276* : 25520–31.

White, C.W., Caspar, B., Vanyai, H.K., Pfleger, K.D.G., and Hill, S.J. (2020). CRISPR-Mediated Protein Tagging with Nanoluciferase to Investigate Native Chemokine Receptor Function and Conformational Changes. *Cell Chem. Biol. 27:* 499–510.

Windwarder, M., Yelland, T., Djordjevic, S., and Altmann, F. (2016). Detailed characterization of the O-linked glycosylation of the neuropilin-1 c/MAM-domain. *Glycoconj. J. 33* : 387–97.

Witmer, A.N., Dai, J., Weich, H.A., Vrensen, G.F.J.M., and Schlingemann, R.O. (2002). Expression of vascular endothelial growth factor receptors 1, 2, and 3 in quiescent endothelia. *J. Histochem. Cytochem.50* : 767–77.

Woolard, J., Bevan, H.S., Harper, S.J., and Bates, D. (2009). Molecular diversity of VEGF-A as a regulator of its biological activity. *Microcirculation 16* : 572–92.

Woolard, J., Wang, W., Bevan, H.S., Qiu, Y., Morbidelli, L., Pritchard-jones, R.O., et al. (2004). VEGF 165b, an Inhibitory Vascular Endothelial Growth Factor Splice Variant: Mechanism of Action , In vivo Effect On Angiogenesis and Endogenous Protein Expression. *Cancer Res. 64* : 7822–35.

FIGURE LEGENDS

Figure 1. **Localisation of VEGFR2 and NRP1 co-expressed in living HEK293T cells** . (a) HEK293T cells expressing HaloTag-VEGFR2 and SnapTag-NRP1 were simultaneously labelled with membrane-impermeant 0.5 μM HaloTag-AlexaFluor488 and 0.5 μM SnapTag-AlexaFluor647 for 30 minutes (37°C). Cells were washed twice in HEPES Buffered Saline Solution (HBSS) containing 0.1% Bovine Serum Albumin (BSA) and incubated at 37°C. Cells were imaged on the LSM710 Confocal Microscope (40X objective). The same cell population were imaged in the presence of vehicle or following treatment with 10 nM unlabelled $VEGF_{165}$b or $VEGF_{165}$a for 60 minutes (37°C). Images show HaloTag-VEGFR2 (green) and SnapTag-NRP1 (magenta), showing regions of spatial overlay in white. Images are representative from 4 independent experiments. (b,c) ImageJ/Fiji software was used to analyse images with channels corresponding to HaloTag-VEGFR2 or SnapTag-NRP1. Co-localisation was quantified based on regions of interest drawn around cells co-expressing both receptors. Mander's Overlap Coefficients represent the proportion of SnapTag-NRP1 in HaloTag-VEGFR2+ regions (b), whereas Pearson's Correlation Coefficients compare the relationship between the intensity of VEGFR2 and NRP1 pixels (c). All coefficient values were pooled from 4 independent experiments, with a total of 97 cells (vehicle), 68 cells ($VEGF_{165}$b) or 54 cells ($VEGF_{165}$a). Coefficients were compared between conditions using a Kruskal-Wallis test and post-Hoc Dunn's multiple comparisons test between vehicle, $VEGF_{165}$b or $VEGF_{165}$a stimulation (* $P< 0.05$).

Figure 2. **Oligomer formation between VEGFR2 and NRP1.** (a,b) HEK293T cells were transiently transfected with a fixed concentration of NanoLuc-VEGFR2 (25 ng cDNA/well) and increasing concentrations of fluorescent acceptor (HaloTag-NRP1 or SnapTag-NRP1, 0-100 ng cDNA/well). All wells were transfected with 125 ng cDNA/well total with empty pcDNA3.1/Zeo vector. NRP1 was labelled with 0.2 μM HaloTag-AlexaFluor488 substrate or 0.2 μM SNAP-Surface AlexaFluor488 substrate for 30 minutes (37°C). Cells were washed twice with HBSS/0.1% BSA then incubated in 10 μM furimazine for 5 minutes (37°C). Emissions from the luminescent donor and fluorescent acceptor receptor were simultaneously monitored by the PHERAstar FS platereader. Data are expressed as (a) mean ± S.E.M. from 5 independent experiments with duplicate wells or (b) individual data points from a representative experiment plotting BRET ratio values against fluorescence emissions (485-520 nm).

Figure 3. **Complementation of a VEGFR2/NRP1 NanoBiT complex** . (a) To determine the optimal orientation of labelling with NanoLuc Binary Technology (NanoBiT) fragments, each receptor was tagged with the 18 kDa fragment (LgBiT) and a smaller 11 amino acid fragment. HiBiT has a higher intrinsic affinity to complement with LgBiT compared to SmBiT (Dixon et al., 2016). HEK293T cells were transiently transfected in 96-well plates with equal amounts of LgBiT-tagged receptor (50 ng cDNA/well) and HiBiT- or SmBiT-tagged receptor (50 ng cDNA/well). Cells were incubated with 10 μM furimazine in HBSS/0.1% BSA for 10 minutes (37°C). Data were normalised to un-transfected cells (0%) and HiBiT-NRP1/LgBiT-VEGFR2 (100%) per experiment. Data are expressed as mean ± S.E.M. from 5 independent experiments (LgBiT-VEGFR2) or 3 independent experiments (LgBiT-NRP1), each with triplicate wells. (b) To compare emissions from individual NanoBiT-tagged receptors relative to a complemented NanoBiT complex, HEK293T cells were transiently transfected in 96-well plates with LgBiT-VEGFR2, HiBiT-NRP1 or SmBiT-NRP1 (50 ng cDNA/well). Dual expression cells expressed a complemented NanoBiT complex (filled bars) whereas single constructs (empty bars) were transfected with 50 ng cDNA/well empty pcDNA3.1/Zeo vector for 100 ng total cDNA/well. Experiments were repeated in 5 independent experiments. Raw emissions were plotted from a representative experiment as mean ± S.E.M. from triplicate wells. (c) Cells expressed a single NanoBiT-tagged construct, in the absence (open bars) or presence (filled bars) of 20 nM purified HiBiT or LgBiT. Data are representative from 5 independent experiments from the same experiment as (b). Raw emissions were plotted as mean ± S.E.M. from triplicate wells. (d) Prevention of NanoBiT complex formation by co-expression of increasing amounts of competing VEGFR2 or NRP1. HEK293T cells were transfected with equal amounts of LgBiT-VEGFR2 (50 ng cDNA/well) and either HiBiT-NRP1 (lined bars) or SmBiT-NRP1 (solid bars) at 50 ng cDNA/well. Cells were also transfected with increasing amounts of HaloTag-NRP1 (0-200 ng cDNA/well), as well as with pcDNA3.1/Zeo empty vector (for 300 ng total cDNA/well). Data were

normalised to un-transfected cells (0%) and the complemented NanoBiT complex in the absence of competing receptor (100%) per experiment. Data are expressed as mean ± S.E.M. from 3 independent experiments, each with triplicate wells. (a-d) Cells were incubated with furimazine (10 μM) in HBSS/0.1% BSA for 10 minutes (37°C). Luminescence emissions (475-505 nm) were measured by the PHERAstar FS platereader.

Figure 4. **Bioluminescence imaging of NanoLuc-VEGFR2, NanoLuc-NRP1 or NanoBiT-complemented VEGFR2-NRP1 complexes.** HEK293T cells were transfected with LgBiT-VEGFR2 (750 ng cDNA/well) and HiBiT-NRP1 (750 ng cDNA/well). Following 24 hours, transfected cells were seeded into 35 mm^2 glass-bottomed dishes. Cells were incubated with furimazine for 10 minutes at 37°C (26 μM for full-length NanoLuc; 104 μM for NanoBiT complex). Cells were imaged live using a widefield Olympus LV200 Bioluminescence Imaging System as described under Methods. Images are representative from 3 independent experiments.

Figure 5. **Characterisation of NFAT signalling from VEGFR2 tagged with LgBiT, HiBiT or SmBiT moieties.** HEK293T cells stably expressed both NFAT-ReLuc2P and either LgBiT-VEGFR2, HiBiT-VEGFR2 or SmBiT-VEGFR2. (a) Cells were serum-starved for 24 hours. On the day of experimentation, cells were stimulated with increasing concentrations of $VEGF_{165}$a for 5 hours and 37°C/5% CO_2. Data were normalised to mean vehicle (0%) or 10 nM unlabelled $VEGF_{165}$a (100%) per experiment. Data are expressed as mean ± S.E.M. from 5 independent experiments with duplicate wells per experiment.

Figure 6. **Saturation binding of $VEGF_{165}$b-TMR and $VEGF_{165}$a-TMR at a HiBiT complex of VEGFR2 and NRP1** . (a) Fluorescent VEGF-A ligand binding was monitored at a defined complex of LgBiT-VEGFR2 and HiBiT-NRP1. In the presence of furimazine, individual receptors do not emit luminescence in isolation. Upon NanoBiT complementation, luminescence emissions can excite the tetramethylrhodamine (TMR) in close proximity. NanoBiT therefore only acts as a luminescent donor when VEGFR2 and NRP1 are in complex. (b,c) HEK293T cells were transfected in 6-well plates with equal amounts of LgBiT-VEGFR2 (750 ng cDNA/well) and HiBiT-NRP1 (750 ng cDNA/well). Following 24 hours, transfected cells were seeded in 96-well plates. On the day of experimentation, cells were incubated with increasing concentrations of $VEGF_{165}$b-TMR (b) or $VEGF_{165}$a-TMR (c). This was performed in the presence or absence of 100 nM $VEGF_{165}$b (b) or $VEGF_{165}$a (c) to determine non-specific binding. Following 60 minutes at 37°C, 10 μM furimazine was added for 10 minutes (37°C). Emissions were measured on the PHERAstar platereader. BRET ratios are expressed as mean ± S.E.M. from 3 independent experiments with duplicate wells.

Figure 7. **Real-time binding of fluorescent VEGF-A isoforms at the NanoBiT complex compared to isolated receptors.** (a) HEK293T cells were transfected in 6-well plates with equal amounts of LgBiT-VEGFR2 (750 ng cDNA/well) and HiBiT-NRP1 (750 ng cDNA/well). Alternatively, cells were transfected with equal amounts of NanoLuc-VEGFR2 or NanoLuc-NRP1 (750 ng cDNA/well) and empty pcDNA3.1/Zeo vector (750 ng cDNA/well). Following 24 hours, transfected cells were seeded in 96-well plates. On the day of experimentation, cells were pre-treated with furimazine (10 μM) and left to equilibrate at 37°C for 10 minutes. (a) Cells expressing the NanoBiT complex (LgBiT-VEGFR2/HiBiT-NRP1) were stimulated with 4 concentrations of $VEGF_{165}$b-TMR added at x=0. Kinetic data were fitted to a global association model with an unconstrained k_{on} from the 90 minute time course. (b) On the same plate, the real-time binding profile of 20 nM $VEGF_{165}$b-TMR was monitored in cells only expressing either NanoLuc-VEGFR2 or NanoLuc-NRP1 (left y axis, grey symbols). This was directly compared to binding of the same concentration of $VEGF_{165}$b-TMR at the LgBiT-VEGFR2/HiBiT-NRP1 NanoBiT Complex (right y axis, red circular symbols). (c) Cells expressing the HiBiT complex were stimulated with 4 concentrations of $VEGF_{165}$a-TMR. Kinetic data were fitted to a global association model without a constrained k_{on} from the initial 20 minutes due to the latter decline in BRET ratio. (d) The real-time binding profile of a saturating concentration of $VEGF_{165}$a-TMR (10 nM) was compared between cells expressing LgBiT-VEGFR2/HiBiT-NRP1 (right y axis, blue circular symbols) to cells only expressing NanoLuc-VEGFR2 or NanoLuc-NRP1 (left y axis, open symbols). For each experiment, emissions were simultaneously measured on the PHERAstar FS platereader every 30 seconds for 90 minutes at 37°C. BRET ratios were baseline-corrected to vehicle at each time point per experimental replicate. In (b) and (d), the x axis was split to highlight the initial association (20 minutes) and long-term

BRET signal (90 minutes). Data represent mean ± S.E.M. from 5 independent experiments with duplicate wells. Derived k_{on}, k_{off} and kinetic pK_d parameters are in Table 1.

Figure 8**. Fluorescent VEGF-A binding kinetics at a NanoBiT VEGFR2/NRP1 complex using split tags with lower intrinsic affinity** . HEK293T cells were transfected in 6-well plates with equal amounts of LgBiT-VEGFR2 (750 ng cDNA/well) and SmBiT-NRP1 (750 ng cDNA/well). Following 24 hours, transfected cells were seeded in 96-well plates. Cells were pre-treated with furimazine (10 μM) and left to equilibrate at 37°C for 10 minutes. (a) Cells were stimulated with 4 concentrations of $VEGF_{165}$b-TMR added at x=0. Kinetic data were fitted to a global association model without a constrained $k_{on}$from the 90 minute time course. For clarity, the 10 nM data set has not been included in the figure. (b) The derived rate constant, k_{obs}, was obtained from exponential association curves fitted for each of the four fluorescent ligand concentrations. These were plotted against $VEGF_{165}$b-TMR concentration and fitted against a linear regression (HiBiT Complex y = 0.0023x + 0.034, R^2 = 0.46; SmBiT Complex y = 0.0026x + 0.01, R^2 = 0.65). (c) Cells were stimulated with 4 concentrations of $VEGF_{165}$a-TMR. Kinetic data were fitted to a global association model without a constrained $k_{on}$from the initial 20 minutes due to the latter decline in BRET ratio. For clarity, the 5 nM data set has not been included in the figure. (d) The derived k_{obs} for each fluorescent ligand at all four concentrations were plotted against each $VEGF_{165}$a-TMR concentration and fit with a linear regression (HiBiT Complex y = 0.0024x + 0.10, R^2 = 0.72; SmBiT Complex y = 0.0025x + 0.09, R^2 = 0.62). Emissions were simultaneously measured on the PHERAstar FS platereader every 30 seconds for 90 minutes at 37°C. BRET ratios were baseline-corrected to vehicle at each time point per replicate. Data represent mean ± S.E.M. from 5 independent experiments with duplicate wells in each independent experiment. Derived k_{on}, k_{off} and kinetic pK_d parameters are in Table 1.

Figure 9. **Ligand binding of $VEGF_{165}$a-TMR at a NanoBiT complex with a binding-dead NRP1 mutant** . (a) $VEGF_{165}$a-TMR ligand binding was monitored at a defined NanoBiT complex between LgBiT-VEGFR2 and a HiBiT-NRP1 VEGF-A binding-dead mutant in the b1 domain. (b) HEK293T cells were transiently transfected in 96-well plates with LgBiT-VEGFR2, HiBiT-NRP1 Y297A or SmBiT-NRP1 Y297A (50 ng cDNA/well). Dual expression cells expressed a complemented NanoBiT complex with the HiBiT or SmBiT tag. Cells also expressed single constructs (empty bars) were transfected with 50 ng cDNA/well empty pcDNA3.1/Zeo vector. Cells were incubated with 10 μM furimazine in HBSS/0.1% BSA for 10 minutes (37°C). Luminescence emissions (475-505 nm) were measured by the PHERAstar FS platereader. Data were normalised to un-transfected cells (0%) and HiBiT-NRP1 Y297A/LgBiT-VEGFR2 (100%) per experiment. Data are expressed as mean ± S.E.M. from 5 independent experiments, each with triplicate wells. (c,d) HEK293T cells were transfected in 6-well plates with equal amounts of LgBiT-VEGFR2 (750 ng cDNA/well) and HiBiT-NRP1 Y297A (750 ng cDNA/well). Following 24 hours, transfected cells were seeded in 96-well plates. (c) On the day of experimentation, cells were incubated with increasing concentrations of $VEGF_{165}$a-TMR in the presence or absence of 100 nM $VEGF_{165}$a to determine non-specific binding. Following 60 minutes at 37°C, 10 μM furimazine was added for 10 minutes (37°C). Emissions were measured on the PHERAstar platereader (550-LP/460-480 nm). BRET ratios are expressed as mean ± S.E.M. from 3 independent experiments with duplicate wells. Derived equilibrium dissociation constants (pK_d) are in the text. (d) Cells were pre-treated with furimazine (10 μM) and left to equilibrate at 37°C for 10 minutes. Cells were incubated with 4 concentrations of $VEGF_{165}$a-TMR. Kinetic data were fitted to a global association model without a constrained k_{on} from the initial 20 minutes. Emissions were simultaneously measured on the PHERAstar FS platereader every 30 seconds for 90 minutes at 37°C. BRET ratios were baseline-corrected to vehicle at each time point per experimental replicate. Data represent mean ± S.E.M. from 5 independent experiments with duplicate wells. Derived k_{on}, k_{off} and kinetic pK_d parameters are noted in the text.

TABLE

Table 1. **Summary of binding parameters derived at the NanoBiT complex for $VEGF_{165}$b-TMR and $VEGF_{165}$a-TMR, compared to published values from receptors expressed alone** .

	Kinetic pK_d	k_{on} ($min^{-1}M^{-1}$)	k_{off} (min^{-1})
$VEGF_{165}$b-TMR	$VEGF_{165}$b-TMR	$VEGF_{165}$b-TMR	$VEGF_{165}$b-TMR
HiBiT Complex	7.81 ± 0.10 (5)	$2.29x10^6$ ± $0.30x10^6$ (5)	0.037 ± 0.007 (5)
SmBiT Complex	8.43 ± 0.17 (5)	$2.94x10^6$ ± $0.55x10^6$ (5)	0.012 ± 0.003 (5)
$VEGF_{165}$a-TMR			
HiBiT Complex	8.83 ± 0.12 (5)	$3.12x10^7$ ± $0.43x10^7$ (5)	0.046 ± 0.007 (5)
SmBiT Complex	8.83 ± 0.31 (5)	$2.83x10^7$ ± $0.69x10^7$ (5)	0.046 ± 0.020 (5)

Parentheses represent the number of independent experiments, each with duplicate wells. Kinetic parameters were derived from a global association fit from the full 90 minute time course ($VEGF_{165}$b-TMR) or the initial 20 minutes ($VEGF_{165}$a-TMR). Experiments with LgBiT-VEGFR2 and HiBiT-NRP1 (HiBiT Complex) are shown in Figure 7a and c. Kinetic experiments with LgBiT-VEGFR2 and SmBiT-NRP1 (SmBiT Complex) are shown in Figure 8a and c.

Figure 1.

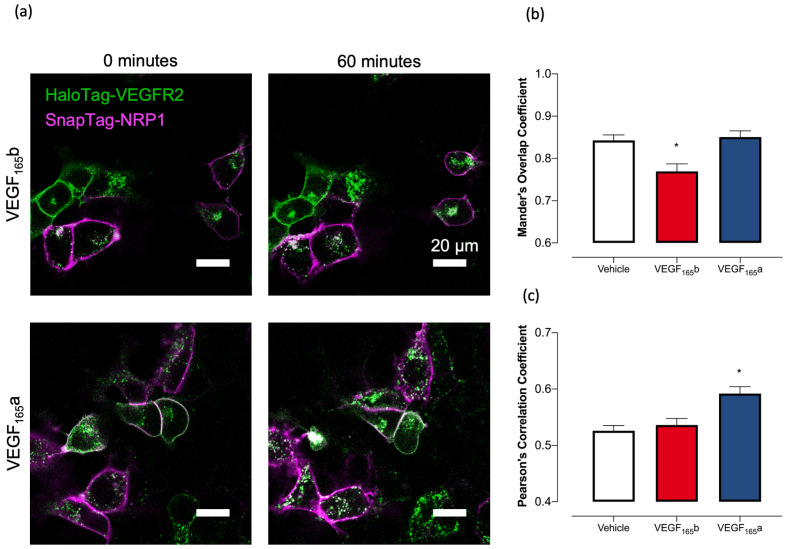

Figure 2.

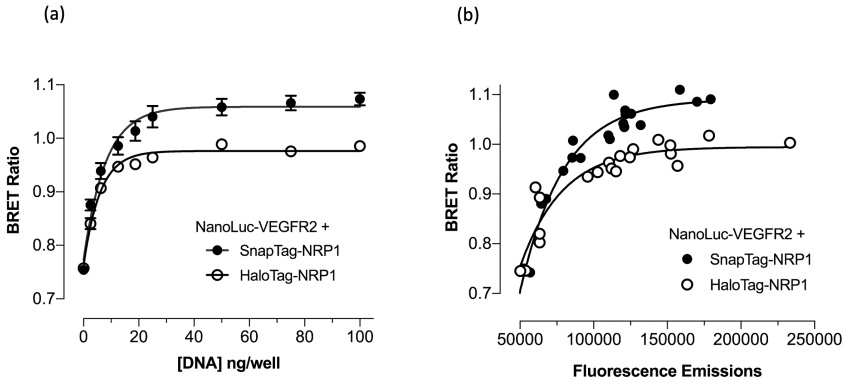

Figure 3.

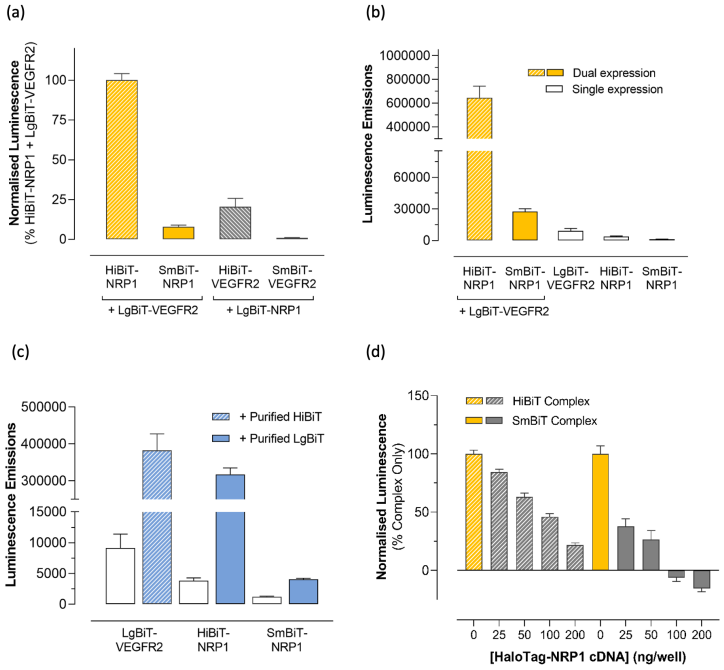

Figure 4.

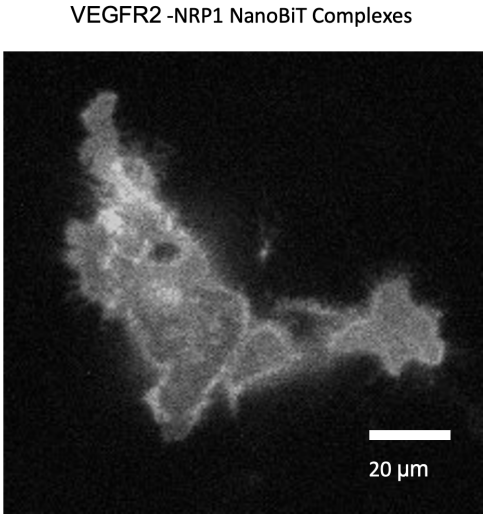

Figure 5.

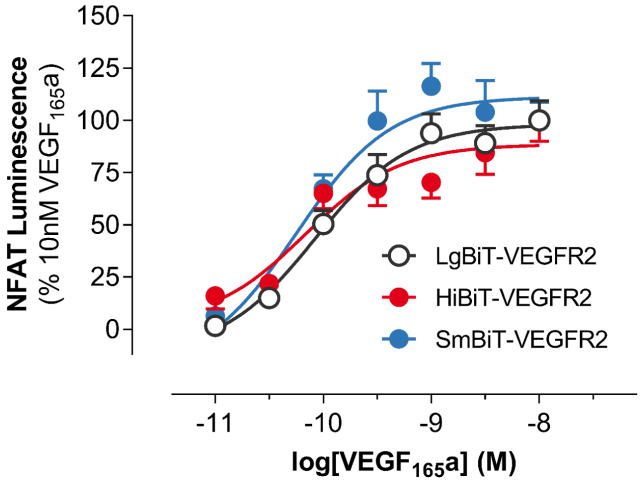

Figure 6.

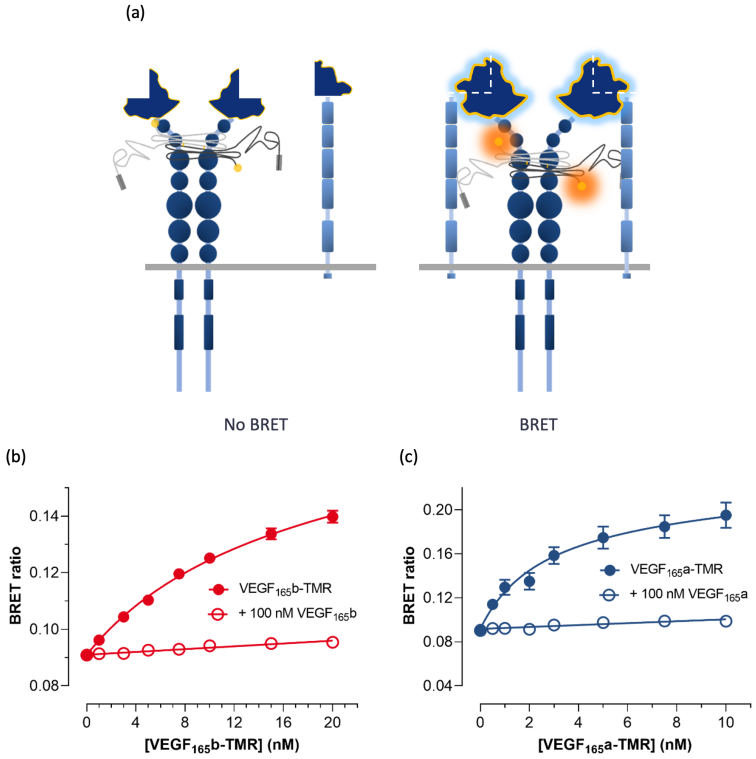

Figure 7.

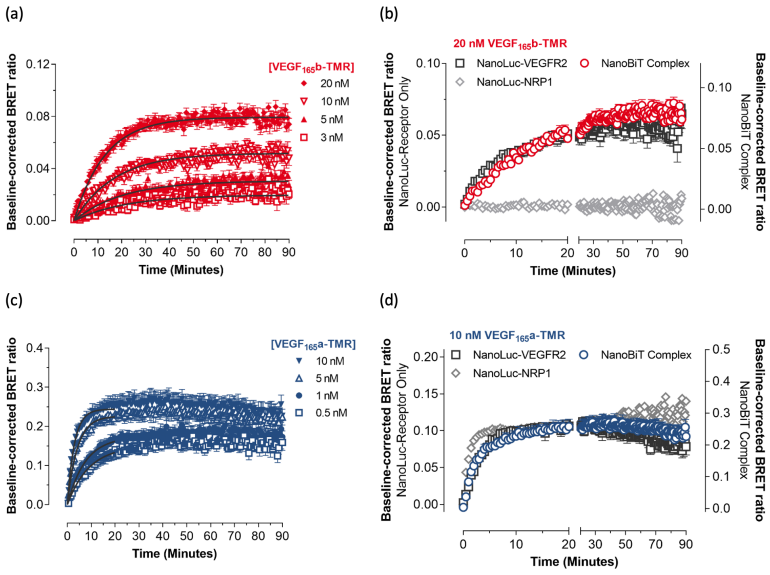

Figure 8.

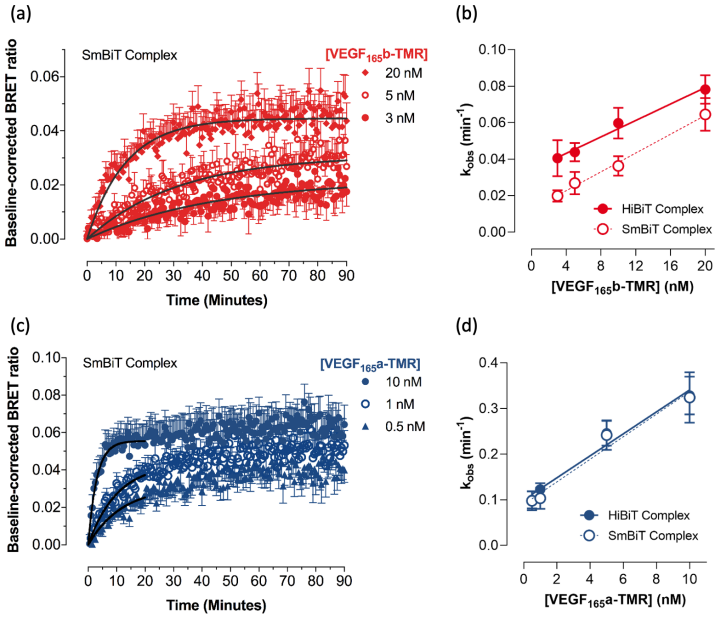

Figure 9.